

Electronic Supplementary Information (ESI)

Knittable energy storing fiber with high volumetric performance made from predominantly MXene nanosheets

Shayan Seyedin,^a Elliard Roswell S. Yanza,^a and Joselito M. Razal*^a

^aDeakin University

Institute for Frontier Materials

Geelong, VIC 3216, Australia

E-mail: joselito.razal@deakin.edu.au

Supplementary experimental

Graphene oxide synthesis

Liquid crystalline (LC) graphene oxide (GO) dispersions were synthesized according to the previously established method.^{1,2} The GO dispersions for fiber spinning applications were prepared by centrifugation of the as-synthesized GO dispersion ($\sim 1.13 \text{ mg mL}^{-1}$) at 7,500 rpm (8,630 g) for 90 min (Beckman J2-MC). The desired concentration was achieved by removing a known volume of the supernatant.

MXene synthesis

Ti₃C₂ MXene was synthesized using the LiF/HCl method by following the two main steps below:

Etching/exfoliation. 1.98 g LiF (98+%, Bio-Scientific) was dissolved in 30 mL of 6 M HCl (37%, Sigma-Aldrich) in a PTFE beaker. 3 g of Ti_3AlC_2 powder (MAX phase, Carbon Ukraine, particle size $< 40 \mu\text{m}$) was slowly added to the solution. The mixture was heated to $40 \text{ }^\circ\text{C}$ and stirred for 45 h in a sealed beaker. The resulting mixture which contained multi-layer MXene (ml-MXene) was diluted for up to 50 times with water (Milli-Q) and then centrifuged (Beckman J2-MC) at 7,500 rpm (8,630 g) for 15 minutes. Washing with centrifugation was repeated at least five more times ($>10 \text{ L}$ of water used) until the supernatant reached a $\text{pH} > 6$. The washed ml-MXene dispersion was then filtered over a $0.22 \mu\text{m}$ PTFE filter membrane, and the ml-MXene residue was dried and stored in a desiccator under vacuum.

Delamination. To obtain few- and/or single-layer Ti_3C_2 MXene flakes, the filtered ml-MXene powder was delaminated using dimethyl sulfoxide (DMSO, Chem-Supply). $\sim 1 \text{ g}$ of the ml-MXene powder was dispersed in $\sim 200 \text{ mL}$ of DMSO and stirred for 18 h at room temperature. The dispersion was then bath sonicated (Unisonics FXP12M, 100 W) for 1 h. Finally, the sonicated dispersion was centrifuged (Beckman J2-MC) at 500 rpm (38 g) for 1 h and the supernatant containing highly delaminated MXene (concentration $\sim 1.02 \text{ mg mL}^{-1}$) was collected.

MXene/GO spinning formulation preparation

We prepared MXene/GO formulations by a sequential addition-centrifugation process. This process involves combining known volumes of MXene and LCGO dispersions, vortex mixing, centrifuging (ThermoScientific Heraeus Multifuge X3R), removing the supernatant, adding known volume of MXene dispersion, and then repeating this mixing-centrifugation-addition process until the desired MXene/GO compositions were attained. We prepared the formulations using this process to maximize the MXene content in the resulting formulation

and achieved a high MXene loading of up to ~88 wt. %. The delaminated MXene dispersions were initially prepared at a relatively low concentration of $\sim 1 \text{ mg mL}^{-1}$ to ensure high delamination of the MXene nanosheets. All dispersions were prepared in DMSO to prevent the oxidation of MXene. Prior to fiber spinning, the MXene/GO dispersions in DMSO were transferred to water by centrifugation and the concentration of the spinning formulation (total solid content) was adjusted to $\sim 10 \text{ mg mL}^{-1}$. Sonication was not used to maintain the GO sheet size and the LC behavior required for fiber spinning.

MXene/GO fiber processing

MXene/GO fibers were fabricated using the wet-spinning approach we have developed previously,³⁻⁸ which is shown schematically in Fig. 1 (in the paper). The spinning formulations were injected into a rotating coagulation bath of acetic acid (glacial, Sigma-Aldrich) using a 23 gauge needle (inner diameter 0.34 mm) with a flow rate of 10 mL h^{-1} . The MXene/GO fibers were produced continuously, collected on a winder without drawing, and then dried in air at room temperature. The reduction of GO in MXene/GO fibers was carried out by immersing the fibers in 5 wt. % hypophosphorous acid (50 wt. % aqueous solution, Sigma-Aldrich) at 60°C for 12 h. Co-knitting the MXene/GO fibers with a commercial nylon yarn (Toplon, Spin Drawn, Denier/Filament 40/24) was carried out using a circular weft knitting machine (Harry Lucas R1-S, head size 1/12", gauge 28, 8 needles).

Characterization

GO sheets on a silanized silicon wafer were investigated under a field emission scanning electron microscope (SEM, JEOL JSM-7800F). Silicon wafers (SiO_2 layer thickness 285 nm) were first silanized by immersing them into a solution of 3-aminopropyltriethoxysilane (Sigma–Aldrich) in water (1:9 v/v) to which a drop of hydrochloric acid (Sigma–Aldrich) was added, and then rinsing them with water. GO sheets were deposited onto the silanized silicon wafers by dipping the wafers into a diluted GO dispersion ($\sim 50 \mu\text{g mL}^{-1}$) and then air-dried. Transmission electron microscopy (TEM, JEOL JEM-2100) with an accelerating voltage of 200 kV was carried out to observe the MXene flakes. The TEM samples were prepared by dipping a carbon-coated copper grid into a diluted MXene dispersion ($\sim 50 \mu\text{g mL}^{-1}$) and then air-dried. The birefringence of MXene/GO dispersions was investigated under a polarizing optical microscope (Nikon Eclipse 80i equipped with a Nikon DS-Ri2 camera) with a 10X objective in bright field transmission mode. Samples were prepared by transferring $\sim 200 \mu\text{L}$ of the dispersion onto a glass slide.

X-ray diffraction (XRD) patterns were recorded with a powder diffractometer (PANalytical X'Pert Powder) using Cu K_α radiation ($\lambda = 1.54 \text{ \AA}$) at a 2θ scan step of 0.013° and 100 s dwelling time. XRD samples were prepared for the MAX phase and ml-MXene by spreading their powders onto a zero XRD diffraction SiO_2 substrate. For the dispersions of MXene, GO and MXene/GO, $\sim 100 \mu\text{L}$ of the dispersion was transferred onto the SiO_2 plate and dried under vacuum for 24 h to obtain samples for XRD analysis.

The morphology of the as-spun MXene/GO fibers was observed by a field emission SEM instrument (JEOL JSM-7800F). Fiber cross-sections were obtained by immersing the fiber in liquid nitrogen and then breaking the frozen fiber. The elemental maps of the MXene/GO fibers were acquired using the energy-dispersive X-ray spectroscopy (EDS) detector (Oxford

Instruments) of the SEM instrument. The diameter of the fibers was measured using an optical microscope (Olympus DP71) for at least 10 points along their length. A tensile testing instrument (Instron 30 kN Tensile Tester) equipped with a 5 N load cell and grips was used to measure the mechanical properties of the fibers (at least 10 samples per fiber). Samples were prepared by attaching the fiber onto a paper frame (10 mm aperture). After mounting the frame on the grips, the paper was cut in the middle and the fiber was stretched at a strain rate of 0.1 mm min⁻¹ (1 % min⁻¹) until failure. The electrical conductivity of the MXene/rGO fibers was measured using an in-house, linear four-point probe cell (probe spacing ~230 μm) under laboratory humidity and temperature conditions. A potentiostat (eDAQ 466) was used to apply different currents (I) between two outer probes and the resulting voltages (V) were measured between the two inner probes using a digital multimeter (Digitech QM1571). Resistance values measured from the I - V curves were used to calculate the electrical conductivity (at least 10 samples per fiber).

The electrochemical properties of the MXene/rGO fiber electrodes were studied in a three-electrode cell consisting of a single fiber as the working electrode, an Ag/AgCl (3 M KCl) reference electrode, a platinum mesh counter electrode and 1 M H₂SO₄ electrolyte. Cyclic voltammetry (CV), galvanostatic charge-discharge (GCD), and electrochemical impedance spectroscopy (EIS) were performed using an electrochemical workstation (BioLogic SP-300). CVs were recorded using scan rates ranging from 2 to 100 mV s⁻¹. GCD tests were performed between the potential limits of 0 to 0.8 V (*vs.* Ag/AgCl). Specific capacitances were calculated using the slopes of the discharge curves from the GCD. The EIS measurements were carried out at open circuit potential (OCP) by applying an alternating-current (AC) voltage with an amplitude of 10 mV in a frequency range of 5 mHz to 5 MHz.

The fiber supercapacitor device was prepared by closely placing two hybrid fibers in parallel on a glass slide and attaching one end of each fiber to a copper tape using silver paste. The fiber electrodes were then coated with a thin layer of polyvinyl alcohol (PVA)/H₂SO₄ gel electrolyte and air dried.

In order to calculate the electrochemical performance of the fiber electrodes (three-electrode setup) and the supercapacitor device (two-electrode setup), the capacitance of the cell (C_{cell}) was first measured from the CV and GCD curves using the Eqs. (1) and (2).

$$C_{cell} = \frac{\int I_{sp} dV}{2v\Delta V} \quad (1)$$

$$C_{cell} = \frac{i_{sp}}{dV/dt} \quad (2)$$

I_{sp} , v , and ΔV in Eq. (1) represent the specific current in the CV curve (normalized according to the volume, mass, area, or length of one electrode), the scan rate, and the potential window (0.8 V), respectively. In Eq. (2), i_{sp} is the discharge current and dV/dt is the slope of the GCD discharge curve.

The specific capacitances of the single fiber electrodes were calculated from the Eq. (3) for the three-electrode setup and from the Eq. (4) for the two-electrode setup.

$$C_{electrode} = C_{cell} \quad (3)$$

$$C_{electrode} = 2C_{cell} \quad (4)$$

The energy density (E) and power density (P) of the fiber supercapacitor device (based on two-electrode) were calculated from the GCD curves of the device using the Eqs. (5) and (6) respectively.

$$E = \frac{1}{2} C_{cell} (\Delta V - iR_{drop}) \quad (5)$$

$$P = \frac{E}{t_{discharge}} \quad (6)$$

The relationship between the current (i) and scan rate (v) at each voltage (V) can be represented by Eq. 7, in which the constants k_1 and k_2 describe the pseudocapacitance and diffusion-limited contributions to the total capacitance.⁹ We measured the pseudocapacitance contribution to the total capacitance of the hybrid fiber by fitting the CV data using Eq. 7.

$$i(V) = k_1 v^{1/2} + k_2 v \quad (7)$$

Supplementary results and discussion

Validation of MXene synthesis

We validated the synthesis of MXene by a series of characterization after each synthesis step, as follows. We first etched the aluminum layer from the Ti_3AlC_2 MAX phase to produce multilayer MXene (ml-MXene). We confirmed complete etching has occurred by SEM and

XRD analyses. From the SEM images, we found that the ml-MXene comprised of separated layered structure (Fig. S1b), which differed from the closely packed morphology of the parent MAX phase (Fig. S1a). XRD analysis showed that the prominent peak for the MAX phase at $2\theta \sim 39^\circ$ is no longer present in ml-MXene (Fig. S1e) suggesting successful etching of the aluminum layer. Also after the etching process, all (00*l*) peaks shifted to lower 2θ indicating the increase in the interlayer spacing. Specifically, the (002) peak for MAX phase downshifted from $2\theta \sim 9.5^\circ$ to $\sim 6.5^\circ$ in the ml-MXene sample, and also increased in intensity and sharpness. Except for the (002) peak, all other peaks broadened and decreased in intensity.

The ml-MXene powder was then sonicated in DMSO for 1 hour and centrifuged to collect the delaminated MXene (d-MXene) dispersion, as shown in Fig. S1d. TEM characterizations confirmed the delamination of MXene flakes into single and a few layers (Fig. S1c). The lateral dimensions of the MXene sheets were found to be in the range of a few hundreds of nanometers to several micrometers. The selected area electron diffraction (SAED) pattern of the d-MXene flake indicated the presence of a single crystal hexagonal lattice with a *d*-spacing of $\sim 2.57 \text{ \AA}$ for the (100) diffraction. In XRD, the intensity of all ml-MXene peaks decreased except for the (002) peak that became even more prominent and sharper in d-MXene (Fig. S1e) further confirming successful delamination.

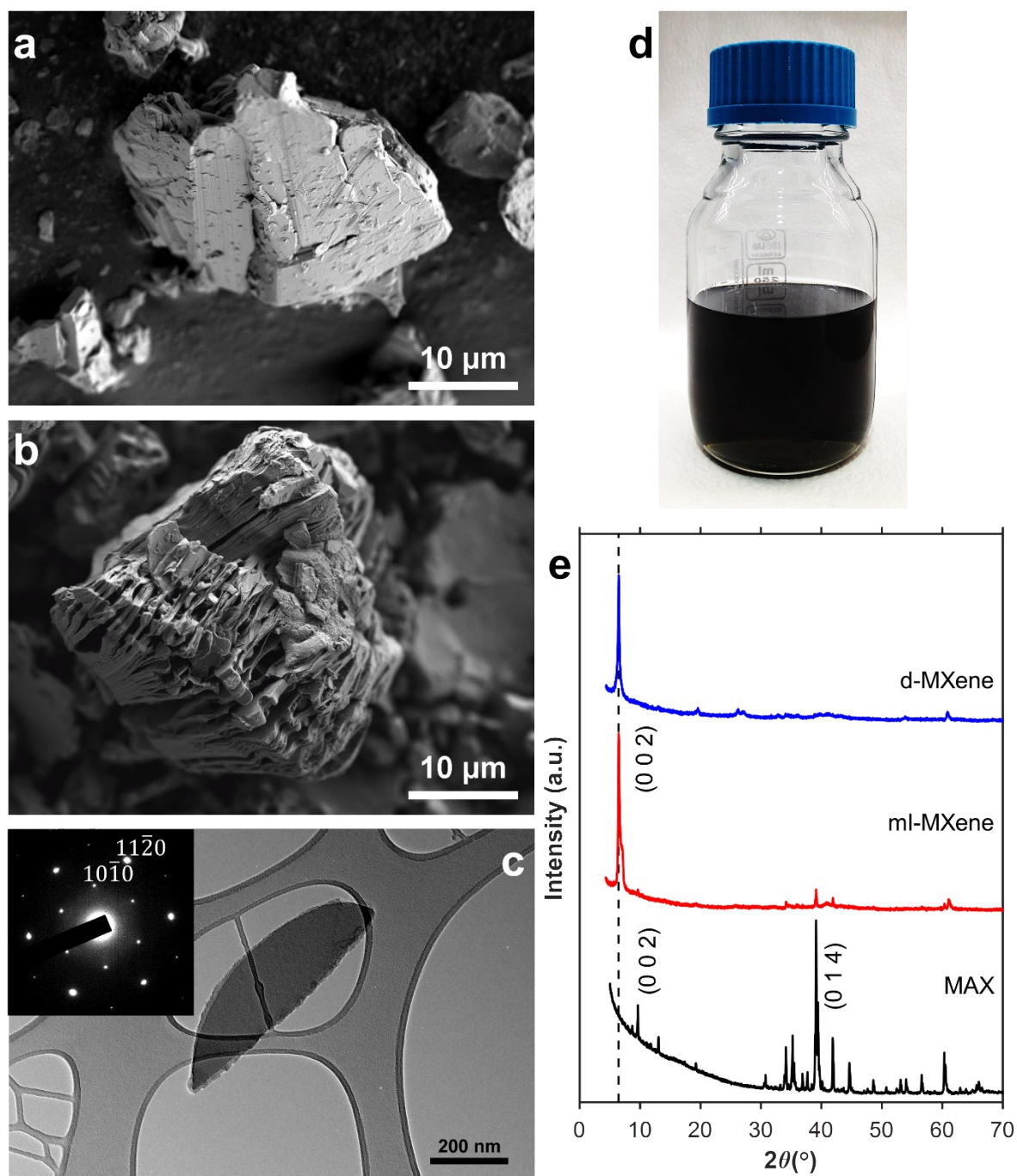


Fig. S1 MXene synthesis and structural characterization. SEM images of (a) Ti_3AlC_2 MAX phase before etching and (b) ml-MXene after etching showing the accordion-like structure. (c) TEM image of a d-MXene. The inset in (c) is the selected area electron diffraction (SAED) pattern of the flake. (d) photograph of d-MXene dispersion in DMSO with the concentration of $\sim 1.02 \text{ mg mL}^{-1}$. (e) XRD spectra of MXene at different stages of synthesis.

Investigations on spinnability and fiber formation

Pure MXene formulations were not spinnable but the addition of LCGO even at low concentration has afforded spinnability to the hybrid formulations. The spinnability tests were conducted by injecting the spinning formulation through a needle into a coagulation bath using the experimental set-up shown in Fig. 1 (in the paper). In this set-up, a fiber forms due to the colloidal interactions and/or solvent exchange from the formulation into the bath and vice versa. When we used 10 wt. % CaCl_2 in 50 vol. % water/ethanol mixture as coagulation bath, the fibers produced at MXene loadings higher than ~3 wt. % could not be collected easily from the coagulation bath. The fibers broke frequently and prevented the collection and drying of a continuous fiber. The spinnability was enhanced significantly when the coagulation bath was changed to glacial acetic acid. This coagulation bath has enabled continuous spinning, collection and drying of all spinning formulations investigated. The strength of the fibers using a spinning formulation with very high MXene loading of ~88 wt. % is demonstrated when approximately 1 meter of fiber was directly pulled out from the bath without breaking, as shown in Fig. S2. This fiber did not need a separate washing step, in contrast to fibers produced using CaCl_2 bath, which needed washing baths to remove the residual CaCl_2 .

When CaCl_2 was used as the coagulant, fibers from pure GO formulations could be produced easily because of the effective ionic cross-linking of the oxygen-containing functional groups on the GO sheets. However, when MXene was added to the spinning formulation, the spinnability decreased. This suggested that the MXene flakes hindered the cross-linking between the GO sheets. In the case of an acetic acid coagulant, the mechanism of fiber formation was solely based on precipitation. This precipitation process held the GO and MXene flakes together, possibly through hydrogen bonding and van der Waals attractions, resulting in the continuous spinning of strong MXene/GO fibers. We also observed that the shape of the fiber cross section differed with increasing MXene loading. In this case, the

interplay between the formulation composition and the coagulation bath composition became important. The irregular cross-section shape of the pure GO fiber suggested that the rate of coagulation of the spinning formulation *i.e.* the extraction rate of water from the formulation by acetic acid was faster than when MXene was present in the formulation. Spinning formulations with increasing MXene loading led to a near circular cross-section, which suggests that differences in surface properties of GO and MXene influence the coagulation rate. Another possible reason for improved circularity with increasing MXene loading is the confinement of MXene flakes within the GO gallery (as observed in the SEMs), which led to more compact fiber structure.



Fig. S2 Digital photograph of a wet-spun MXene/GO fiber (MXene ~88 wt.%). The hybrid fiber could be easily taken out of the coagulation bath without breaking.

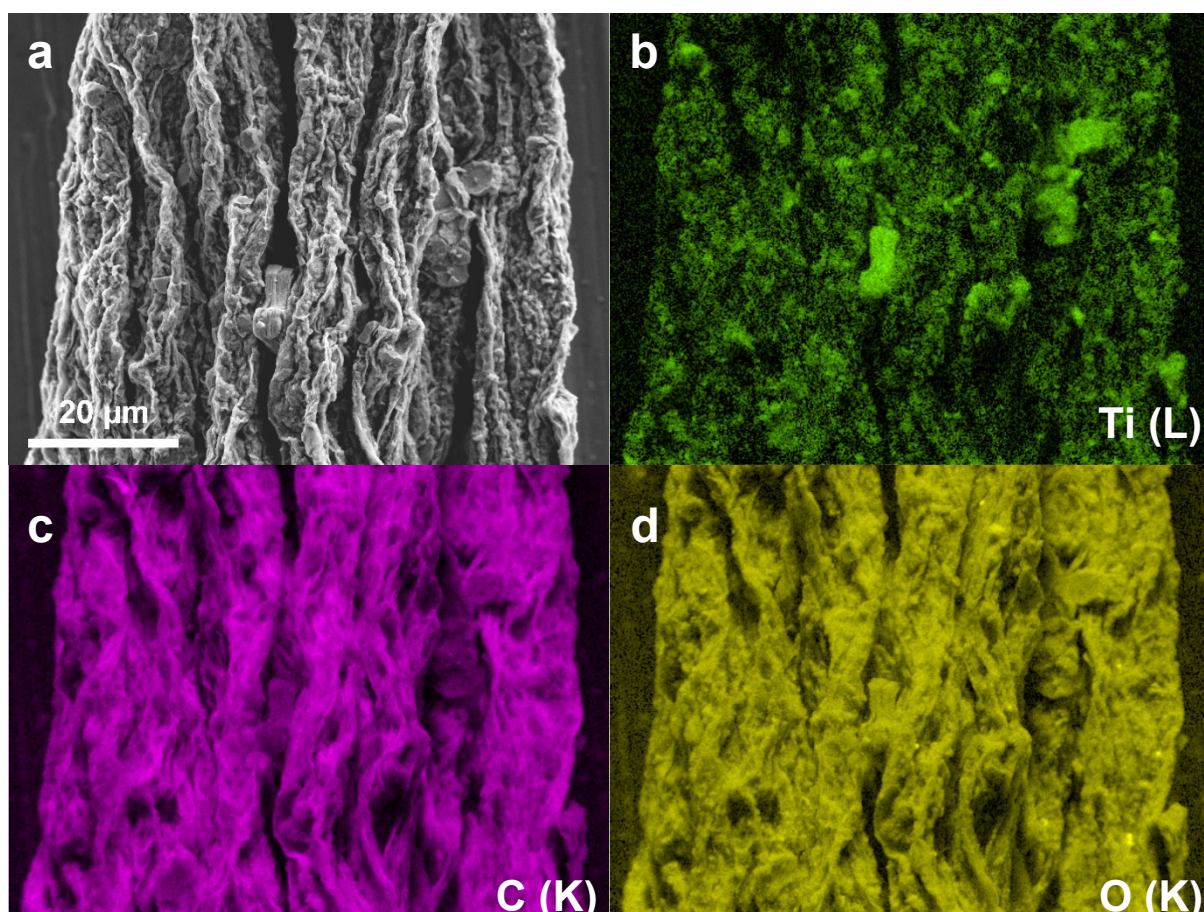


Fig. S3 Elemental mapping of the MXene/GO fiber with the MXene loading of 38.4 wt.% obtained from energy-dispersive X-ray spectroscopy (EDS). (a) SEM of the selected area of the fiber, (b) Ti (L), (c) C (K), and (d) O (K) maps of (a).

Electrochemical performance of MXene/rGO hybrid fibers

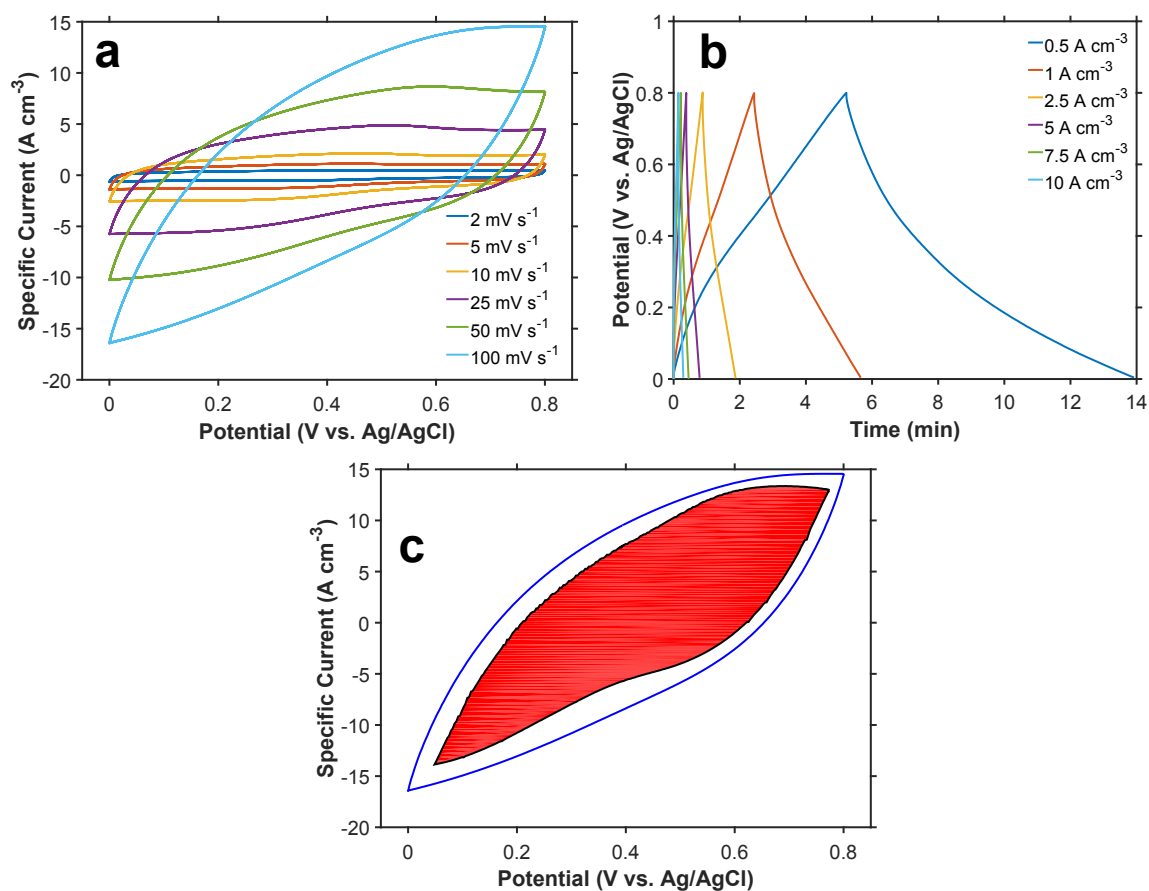


Fig. S4 Electrochemical performance of single MXene/rGO fiber (MXene loading of ~88 wt. %) electrode in a three-electrode setup with 1 M H₂SO₄ electrolyte. (a) cyclic voltammetry (CV) curves at different scan rates. (b) galvanostatic charge/discharge (GCD) curves at various current densities. (c) CV curve at the scan rate of 100 mV s⁻¹ showing the pseudocapacitance contribution with region filled in red.

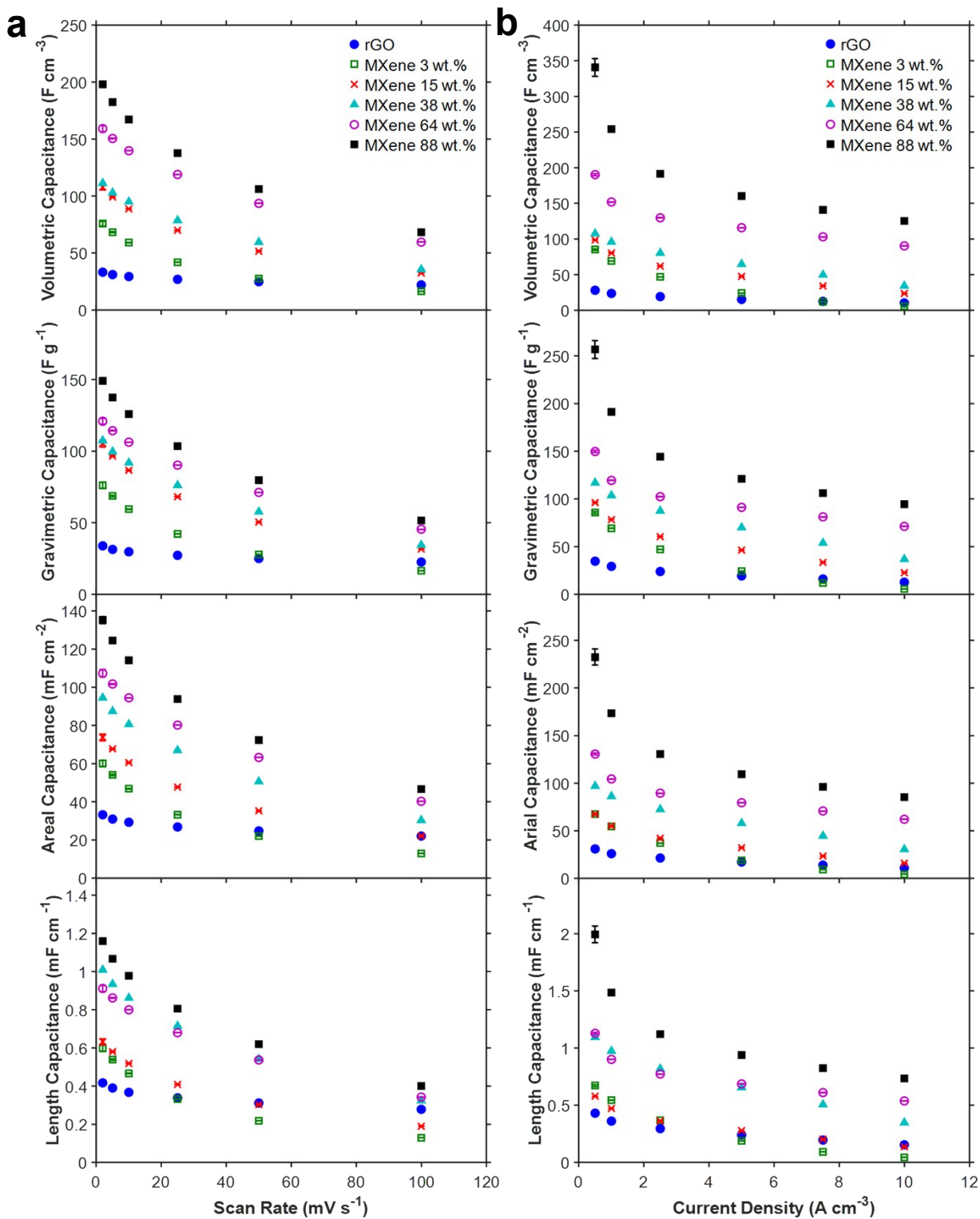


Fig. S5 Volumetric, gravimetric, areal, and length capacitances of single MXene/rGO hybrid fibers at different MXene loadings calculated based on (a) CV and (b) GCD experiments using a three-electrode setup in 1 M H_2SO_4 electrolyte.

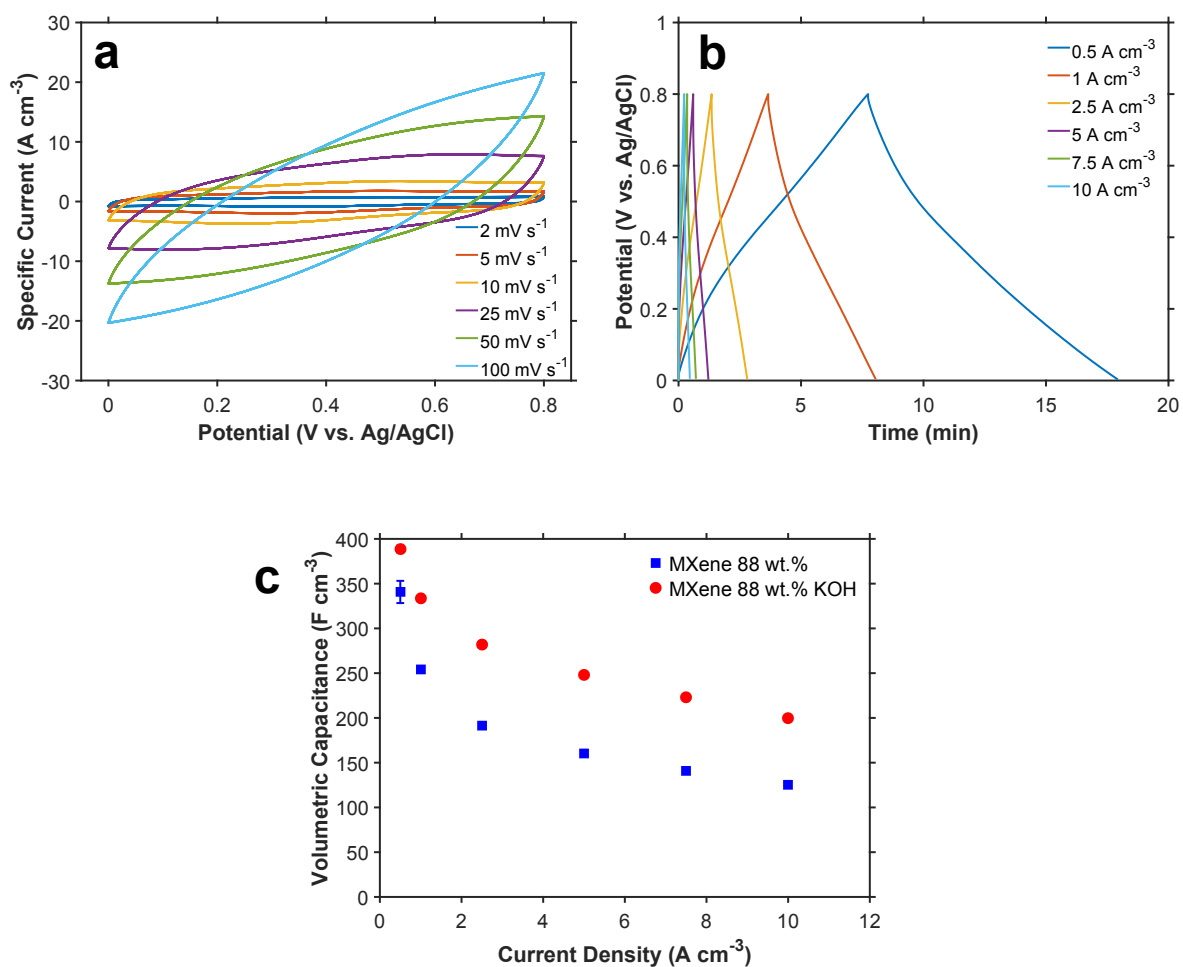


Fig. S6 Electrochemical performance of single MXene/rGO fiber (MXene loading of ~88 wt. %) electrode after wetting with KOH (6 M) tested in a three-electrode setup with 1 M H_2SO_4 electrolyte. (a) CV curves at different scan rates. (b) GCD curves at various current densities. (c) effect of KOH wetting on volumetric capacitance of single MXene/rGO hybrid fiber (MXene loading of ~88 wt. %) at different current densities.

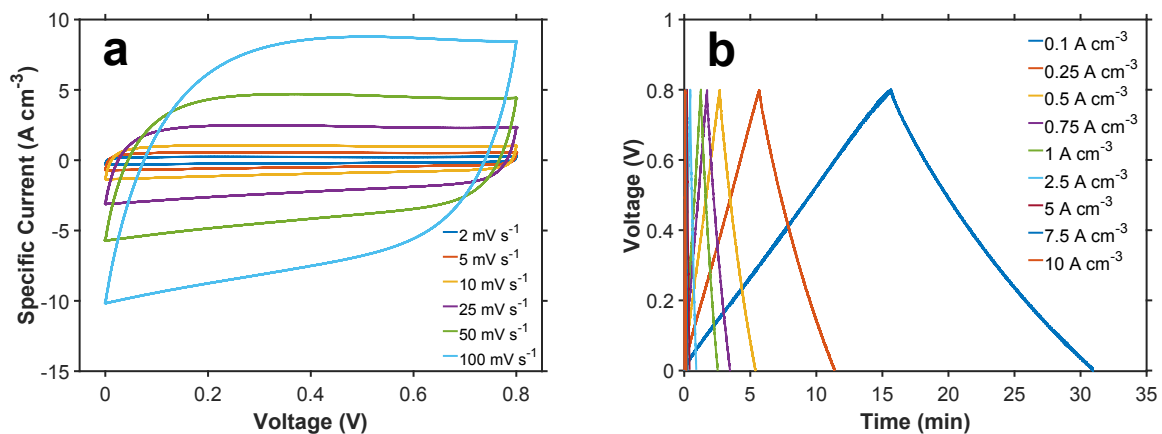


Fig. S7 Electrochemical performance of fiber supercapacitor device made of two MXene/rGO fibers (MXene loading of ~88 wt. %) in with PVA/ H_2SO_4 solid-state electrolyte. (a) CV curves at different scan rates, (b) GCD curves at various current densities.

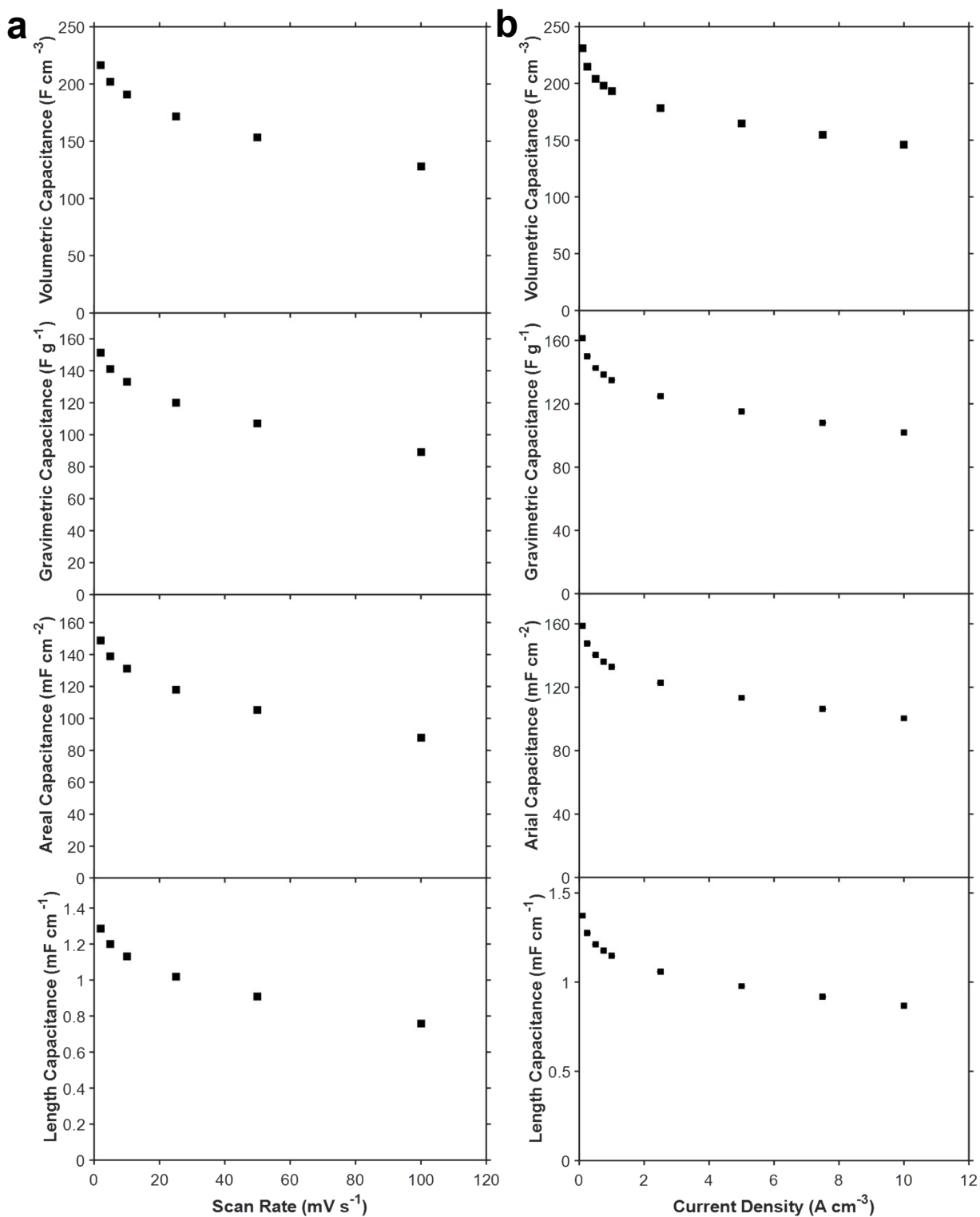


Fig. S8 Volumetric, gravimetric, areal, and length capacitances of the MXene/rGO hybrid fiber electrode (MXene loading of ~88 wt. %) measured from (a) CV and (b) GCD experiments using a two-electrode setup in PVA/H₂SO₄ solid-state electrolyte.

Table S1 Comparison of the electrochemical performance of MXene/rGO hybrid fiber supercapacitor with literature.

Electrode	Setup	σ (S cm ⁻¹)	Y (GPa)	T (MPa)	ε (%)	ΔV (V)	C_A (mF cm ⁻²)	I_A (mA cm ⁻²)	C_V (F cm ⁻³)	I_V (A cm ⁻³)	C_G (F g ⁻¹)	I_G (A g ⁻¹)	Stability	E_A (μ W cm ⁻²)	P_A h (μ W cm ⁻²)	E_V (mW cm ⁻³)	P_V h (mW cm ⁻³)	E_G (W kg ⁻¹)	P_G h (W kg ⁻¹)	Ref	
MXene/rGO hybrid fibre 88 wt. % MXene	H ₂ SO ₄ (Electrode) PVA/H ₂ SO ₄ (Parallel)	72.3	11.3	132.5	2.9	0 – 0.8 vs Ag/AgCl	232.5 85.5	0.34 6.83	340.7 125.3	0.5 10	256.7 94.4	0.38 7.53	~100% 20,000	3.5 1.6	14 1164	5.1 2.3	20 1693	3.6 1.6	14 1183	This work	
SWCNT/rGO fibre	H ₂ SO ₄ (Electrode) PVA/H ₃ PO ₄ (Parallel)	102		84		0 – 1 vs Ag/AgCl			304.8 169.6	0.07 4.41			93% 10,000			6.2 3.0	14 1100			10	
rGO@CMC coaxial fibre	PVA/H ₃ PO ₄ (Twisted)	~70 ^a		73-116	8-10	0 – 0.8	127 12 ^a	0.1 1 ^a	114 9.7 ^a												11
rGO/CNT@CMC coaxial fibre	PVA/H ₃ PO ₄ (Twisted)					0 – 0.8	177 134 ^a	0.1 1	158 119 ^a				~100% 2,000	3.8 2.1 ^a	20 194 ^a	3.5 2.1 ^a	18 196 ^a				11
rGO/MoS ₂ composite fibre	PVA/H ₂ SO ₄ (Twisted)	1.75				0 – 1			30 ^b 16.5 ^{ab}	0.1 1			~80% ^a 1,000			4.1 ^a 2.3 ^a	21 ^a 187 ^a				12
rGO-coated CNT fibre	PVA/H ₃ PO ₄ (Twisted)	~85 ^a		~400 ^a	~4.5 ^a	0 – 1			68.4 45.3 ^a	0.03 1.2 ^a	126.7		~100% 10,000	3.8 2.5 ^a	25 996 ^a	2.4 1.6 ^a	16 619				13
rGO/SWCNT composite fibre	PVA/H ₃ PO ₄ (Parallel)	210.7	5.3	385.7	11.4	0 – 0.8			38.8 ^b 17.1 ^{ab}	0.05 3.2 ^a			93% 10,000			3.4 0.5 ^a	19 ^a 740 ^a				14
rGO/MoS ₂ incorporated MWCNT fibre	PVA/H ₂ SO ₄ (Parallel)	300 ^c				0 – 0.8			6.2 ^{ab} 3.8	0.07 2						0.5 ^a 0.3 ^a	38 ^a 1020 ^a				15
rGO/MoS ₂ incorporated MWCNT fibre	PVA/H ₂ SO ₄ (Parallel asymmetric)					0 – 1.4			5.2 ^b 3.58 ^b	0.16 3.3			~100% 7,000			1.6 ^a 0.9 ^a	38 ^a 2305 ^a				15
rGO coaxial fibre	PVA/H ₂ SO ₄ (Coaxial)	60				0 – 0.8	208.4 122.9	1.10 13.81	231.1 136.3		184.9 109.0	0.49 6.13	~100% 10,000	14.4 ^d 6.4 ^d	346 ^d 3506 ^d	16.0 ^d 7.1 ^d	384 ^d 3889 ^d	12.8 ^d 5.7 ^d	307 ^d 3111 ^d		16
rGO/Ni coated cotton yarn	Na ₂ SO ₄ (Electrode) PVA/LiCl (Twisted)			~55 ^a	~8 ^a	0 – 0.8			292.3 30.2 ^a	0.09 3.52 ^a		311	82% 10,000			12.3 ^e 1.3 ^e	34 ^e 1387 ^e				17
rGO fibre	H ₂ SO ₄ (Electrode) PVA/H ₂ SO ₄ (Parallel)	9.7	6.9	157	2.8	-0.5 – 0.5 vs MSE	119 61.9	0.09 0.85	340 178	0.244 2.44	279 146	0.2 2	92% 1,000			7.0 1.1 ^a	58 372 ^a	5.8	47		18
MnO ₂ -deposited SWCNT fibre	PVA-LiCl (Parallel)	~150	23 ^s	225 ^s	2 ^s	0 – 1			156		152.4 16.0	0.2 8	116 10,000			11.7 ^e 4.8 ^{ae}	168 ^e 6455 ^{ae}	14.1 ^e	202 ^e		19
rGO/MoS ₂ hybrid fibre	PVA-H ₃ PO ₄ (Parallel)	~10 ^a		294	~4	0 – 1	598		368	0.1	191.6 ^a 114.5 ^a	0.1 1	~80% ^a 8,000			12.8					20
MnO ₂ coated Vertically	Na ₂ SO ₄ (Electrode)					-0.2 – 0.8 vs			246 56.8 ^a	2 ^f 100 ^f			96% 10,000			5.7 ^h 2.3 ^{ah}	69 ^{ah} 1010 ^{ah}				21

orientated GO PVP/Na₂SO₄
nanoribbons fibre (Parallel)

SCE

^a Measured from the graph

^b Device

^c Electrical conductivity of pristine MWCNT fibre

^d The energy density and power density values were reported in terms of single electrode. Since the mass of sheath was reported to be equal to the mass of core, the energy density and power density of the device can be calculated by dividing the reported values by a factor of 4.

^e The energy density and power density values were reported in terms of single electrode and can be calculated for the device by dividing the reported values by a factor of 4.

^f mV s⁻¹ based on cyclic voltammetry

^g Mechanical properties are for pristine CNT fibres

^h The whole device volume (based on the device volume including two fibres and the surrounding electrolyte)

References

- 1 R. Jalili, S. H. Aboutalebi, D. Esrafilzadeh, K. Konstantinov, S. E. Moulton, J. M. Razal and G. G. Wallace, *ACS Nano*, 2013, **7**, 3981–3990.
- 2 R. Jalili, S. H. Aboutalebi, D. Esrafilzadeh, R. L. Shepherd, J. Chen, S. Aminorroaya-Yamini, K. Konstantinov, A. I. Minett, J. M. Razal and G. G. Wallace, *Adv. Funct. Mater.*, 2013, **23**, 5345–5354.
- 3 R. Jalili, J. M. Razal, P. C. Innis and G. G. Wallace, *Adv. Funct. Mater.*, 2011, **21**, 3363–3370.
- 4 R. Jalili, J. M. Razal and G. G. Wallace, *J. Mater. Chem.*, 2012, **22**, 25174.
- 5 R. Jalili, J. M. Razal and G. G. Wallace, *Sci. Rep.*, 2013, **3**, 3438.
- 6 M. Z. Seyedin, J. M. Razal, P. C. Innis and G. G. Wallace, *Adv. Funct. Mater.*, 2014, **24**, 2957–2966.
- 7 M. Z. Seyedin, J. M. Razal, P. C. Innis, R. Jalili and G. G. Wallace, *Adv. Funct. Mater.*, 2015, **25**, 94–104.
- 8 S. Seyedin, M. S. Romano, A. I. Minett and J. M. Razal, *Sci. Rep.*, 2015, **5**, 14946.
- 9 V. Augustyn, P. Simon and B. Dunn, *Energy Environ. Sci.*, 2014, **7**, 1597.
- 10 D. Yu, K. Goh, H. Wang, L. Wei, W. Jiang, Q. Zhang, L. Dai and Y. Chen, *Nat. Nanotechnol.*, 2014, **9**, 555–562.
- 11 L. Kou, T. Huang, B. Zheng, Y. Han, X. Zhao, K. Gopalsamy, H. Sun and C. Gao, *Nat. Commun.*, 2014, **5**, 3754.

- 12 G. Sun, J. Liu, X. Zhang, X. Wang, H. Li, Y. Yu, W. Huang, H. Zhang and P. Chen, *Angew. Chemie Int. Ed.*, 2014, **53**, 12576–12580.
- 13 B. Wang, X. Fang, H. Sun, S. He, J. Ren, Y. Zhang and H. Peng, *Adv. Mater.*, 2015, **27**, 7854–7860.
- 14 Y. Ma, P. Li, J. W. Sedloff, X. Zhang, H. Zhang and J. Liu, *ACS Nano*, 2015, **9**, 1352–1359.
- 15 G. Sun, X. Zhang, R. Lin, J. Yang, H. Zhang and P. Chen, *Angew. Chemie Int. Ed.*, 2015, **54**, 4651–4656.
- 16 X. Zhao, B. Zheng, T. Huang and C. Gao, *Nanoscale*, 2015, **7**, 9399–9404.
- 17 L. Liu, Y. Yu, C. Yan, K. Li and Z. Zheng, *Nat. Commun.*, 2015, **6**, 7260.
- 18 S. Chen, W. Ma, Y. Cheng, Z. Weng, B. Sun, L. Wang, W. Chen, F. Li, M. Zhu and H.-M. Cheng, *Nano Energy*, 2015, **15**, 642–653.
- 19 Z. Lu, Y. Chao, Y. Ge, J. Foroughi, Y. Zhao, C. Wang, H. Long and G. G. Wallace, *Nanoscale*, 2017, **9**, 5063–5071.
- 20 B. Wang, Q. Wu, H. Sun, J. Zhang, J. Ren, Y. Luo, M. Wang and H. Peng, *J. Mater. Chem. A*, 2017, **5**, 925–930.
- 21 L. Sheng, T. Wei, Y. Liang, L. Jiang, L. Qu and Z. Fan, *Small*, 2017, **13**, 1–9.